Dalton Transactions

ROYAL SOCIETY OF CHEMISTRY

PAPER

View Article Online
View Journal | View Issue

Open Access Article. Published on 25 November 2020. Downloaded on 2/21/2026 10:56:33 AM.
This article is licensed under a Creative Commons Attribution-NonCommercial 3.0 Unported Licence.

Check for updates

Cite this: *Dalton Trans.*, 2021, **50**, 240

Further synthetic investigation of the general lanthanoid(III) [Ln(III)]/copper(II)/pyridine-2,6-dimethanol/carboxylate reaction system: $\{Cu^{II}_5Ln^{III}_4\}$ coordination clusters (Ln = Dy, Tb, Ho) and their yttrium(III) analogue†

Despina Dermitzaki,[a,b] Catherine P. Raptopoulou, [b] Vassilis Psycharis, [b] Albert Escuer, [c] Spyros P. Perlepes,*[a,d] Julia Mayans [e]*e and Theocharis C. Stamatatos [a,d]*

In addition to previously studied $\{Cu^{II}_3Gd_6\}$, $\{Cu^{II}_8Gd_4\}$, $\{Cu^{II}_{15}Ln_7\}$ and $\{Cu^{II}_4Ln_8\}$ coordination clusters (Ln = trivalent lanthanide) containing pdm^{2-} or $Hpdm^{-}$ ligands (H_2pdm = pyridine-2,6-dimethanol) and ancillary carboxylate groups (RCO_2^-), the present work reports the synthesis and study of three new members of a fifth family of such complexes. Compounds $[Cu_5Ln_4O_2(OMe)_4(NO_3)_4(O_2CCH_2Bu^t)_2(pdm)_4(MeOH)_2]$ (Ln = Dy, **1**; Ln = Tb, **2**; Ln = Ho, **3**) were prepared from the reaction of $Ln(NO_3)_3{\cdot}xH_2O$ (x = 5, 6), $CuX_2{\cdot}yH_2O$ (X = ClO_4, Cl, NO_3; y = 6, 2 and 3, respectively), H_2pdm, $Bu^tCH_2CO_2H$ and Et_3N (2 : 2.5 : 2 : 1 : 9) in MeCN/MeOH. Rather surprisingly, the copper(II)/yttrium(III) analogue has a slightly different composition, *i.e.* $[Cu_5Y_4O_2(OMe)_4(NO_3)_2(O_2CCH_2Bu^t)_4(pdm)_4(MeOH)_2]$ (**4**). The structures of **1**·4MeCN·1.5MeOH and **4**·2MeOH were solved by single-crystal X-ray crystallography. The five Cu^{II} and four Dy^{III} centres in **1** are held together by two μ_5-O^{2-}, four μ-MeO^-, two *syn,syn* $\eta^1{:}\eta^1{:}\mu$ $Bu^tCH_2CO_2^-$, four $\eta^2{:}\eta^1{:}\eta^2{:}\mu_3$ pdm^{2-} (each of these groups chelates a Cu^{II} atom and simultaneously bridges two Dy^{III} atoms through its two $-CH_2O^-$ arms) and two μ-MeOH ligands. The four terminal nitrato groups each chelate ($\eta^1{:}\eta^1$) a Dy^{III} centre. The five Cu^{II} atoms are co-planar (by symmetry) forming a bow-tie arrangement; the four outer Cu^{II} atoms form a rectangle with edges of 3.061(1) and 6.076(1) Å. The four Dy^{III} centres also form a rectangle that lies above and below the plane of the Cu^{II} centres, with edges of 3.739 (1) and 5.328(1) Å. The two strictly planar rectangles are almost perpendicular. Two trigonal bipyramidal μ_5-O^{2-} groups link the perpendicular Cu_5 and Dy_4 frameworks together. The molecule **4** has a very similar structure to that of **1**, differences being the replacement of the two chelating nitrato groups of **1** by two chelating $Bu^tCH_2CO_2^-$ ligands in **4** and the coordination polyhedra of the Ln^{III} and Y^{III} atoms (Snub diphenoids in **1** and biaugmented trigonal prisms in **4**). Dc magnetic susceptibility data (χ_M) on analytically pure samples of **1–3**, collected in the 300–2 K range, indicate that ferromagnetic exchange interactions dominate leading to large spin ground states. The χ_MT *vs.* T data for **4** suggest moderately strong antiferromagnetic $Cu^{II}{\cdots}Cu^{II}$ exchange interactions. Studies of the dynamic magnetic properties of the $\{Cu_5Ln_4\}$ clusters show that **1** behaves as a SMM at zero field and **2** is a very weak field-induced SMM, while **3** exhibits only weak tails in the χ''_M *vs.* T plots at various ac frequencies at zero dc field.

Received 15th October 2020,
Accepted 25th November 2020

DOI: 10.1039/d0dt03582c

rsc.li/dalton

[a]*Department of Chemistry, University of Patras, 26504 Patras, Greece. E-mail: perlepes@upatras.gr, thstama@upatras.gr; Tel: +30 2610 996730, +30 2610 997732*

[b]*Institute of Nanoscience and Nanotechnology, NCSR "Demokritos", 15310 Aghia Paraskevi Attikis, Greece*

[c]*Departament de Química Inorgànica i Orgànica, Secció Inorgànica and Institut de Nanociència i Nanotecnologia (IN2UB), Universitat de Barcelona, Martí i Franquès 1-11, 08028-Barcelona, Spain*

[d]*Institute of Chemical Engineering Sciences, Foundation for Research and Technology – Hellas (FORTH/ICE – HT), Platani, P.O. Box 1414, 26504 Patras, Greece*

[e]*Instituto de Ciencia Molecular (ICMol), Universidad de Valencia, Catedrático José Beltran 2, 46980 Paterna, Spain. E-mail: julia.mayans@uv.es*

†Electronic supplementary information (ESI) available: Various structural plots for **1**·4MeCN·1.5MeOH and **4**·2MeOH (Fig. S1–S7), Argand plots for **1** (Fig. S8), and crystallographic data for **1**·4MeCN·1.5MeOH and **4**·2MeOH (Table S1) and short IR discussion. CCDC 2038607 and 2038608. For ESI and crystallographic data in CIF or other electronic format see DOI: 10.1039/d0dt03582c

This journal is © The Royal Society of Chemistry 2021

Open Access Article. Published on 25 November 2020. Downloaded on 2/21/2026 10:56:33 AM.
This article is licensed under a Creative Commons Attribution-NonCommercial 3.0 Unported Licence.

Introduction

The chemistry of mixed 3d/4f-metal molecular compounds and materials is not new.[1–7] The synthesis of 3d/4f-metal complexes has been a "hot" topic in molecular inorganic chemistry because of their potential applications in several fields such as luminescence,[8,9] near-IR chiroptical sensors,[10] non-linear optical materials,[11] molecular adsorption,[12] catalysis[13] and various aspects of Molecular Magnetism.[14–24]

In the beginning of the present century, there was an intense re-ignition of research interest in the synthesis of polynuclear (or polymetallic) coordination clusters containing both 3d- and 4f-metal ions. The intense activity originated from two major sources: single-molecule magnetism[25,26] and molecular cooling;[27,28] we briefly comment only on the former, because this area is related to the present work. The discovery in the early 1990s that well-isolated magnetic molecules containing 3d-metal ions can exhibit slow paramagnetic relaxation reminiscent of single-domain magnetic particles[27–30] sparked an explosive interest in the magnetism community. The so named Single-Molecule Magnets (SMMs) were originally polynuclear 3d-metal clusters that exhibit a large overall ground-state spin value and a significant uniaxial magnetic anisotropy.[25,31] Until ~2000, the search for new examples of SMMs focused mainly on clusters containing 3d-metal ions. Since the barrier to magnetization reversal (U_{eff}) is related to both the overall spin and the magnitude of the anisotropy in the cluster, researchers began slowly after 2000 to investigate the incorporation of Ln^{III} ions in such systems,[32–35] since they often have high spin as well as significant anisotropy arising from strong spin–orbit contributions. In addition, the 3d–4f exchange interactions (the study of which has been pioneered by the Gatteschi and Winpenny groups) are stronger than the 4f–4f ones suppressing quantum tunneling of magnetization. Thus, much of the current polynuclear SMM research has been shifted toward 3d/4f-metal clusters and hundreds of such SMMs have been prepared and characterized.[36–42] The most preferred Ln^{III} ions for such studies are Tb^{III}, Dy^{III}, Ho^{III} and Er^{III}, since it has been shown that mononuclear complexes containing these Ln^{III} ions can display hysteresis loops in magnetization *vs.* field studies.[34]

From the synthetic inorganic chemistry viewpoint, methods to combine 3d- and 4f-metal ions within a coordination cluster are highly desirable. There is one strategy and one more empirical route for the synthesis of 3d/4f-metal clusters. The strategy is based on the "metal complexes as ligands" approach.[43–45] Mononuclear or dinuclear 3d-metal complexes with uncoordinated O-donor groups can be used as starting materials; such complexes can be considered as "ligands" (metalloligands) and further react with the strongly oxophilic Ln^{III} (Ln = lanthanoid) ions. Alternatively, the metalloligands can be mononuclear or dinuclear Ln^{III} complexes with uncoordinated N-donor sites which further react with the 3d-metal ions. The route which is most often used, is based on "one-pot" procedures.[43–45] These require a mixture of the appropriate 3d- and 4f-metal "salts" (usually with inorganic anions, *e.g.* Cl^-, NO_3^-, ClO_4^-, BF_4^-, $CF_3SO_3^-$,...) and a carefully selected organic ligand possessing distinct coordination compartments ("pockets") for preferential binding of the 3d- and the 4f-metal ion. Sometimes the 3d-metal ions are used in the form of small clusters to ensure high nuclearity in the final heterometallic products. A variation of the "one-pot" approach is the "assisted self-assembly" when the introduction of a second suitable organic co-ligand (*e.g.* a simple carboxylate group) is essential to assist the self-assembly process and often to increase the nuclearity of the heterometallic cluster.[36] Primary organic ligands used include polydentate Schiff bases, oximes, 2-pyridyl alcohols, amino polyalcohols, pyridylcarbonyl amines and amino acids.[36–45] The Hard–Soft Acid–Base (HSAB) model plays an important role in the "one-pot" route facilitating selective heterometallic coordination.[46] For example, Ln^{III} ions are hard acids, whereas the late divalent 3d metals (*e.g.* Co^{II}, Ni^{II}, Cu^{II}) are borderline acids; thus, the former can bind strongly to hard O-donors, while the latter prefer the less hard N-sites or purely soft bases.[45]

We have been involved in a research programme aiming to prepare, characterize and study the magnetic properties of Cu^{II}/Ln^{III} coordination clusters. Such clusters currently attract the intense interest of the inorganic chemistry community.[47–50] We have been using the "assisted self-assembly" variation of the "one-pot" approach by employing pyridine-2,6-dimethanol (H_2pdm) as the primary organic ligand and simple carboxylate ions (RCO_2^-) as co-ligands.[51,52] The anionic forms of H_2pdm are well-explored ligands in transition-metal[53–56] and lanthanoid(III)[57–59] cluster chemistry, having yielded complexes with aesthetically pleasing structures and interesting properties. On the contrary, their use in 3d/4f-metal chemistry has been limited.[51,52,60–64] The tridentate pdm^{2-} anion is not a compartmental ligand. However, it provides a stable tridentate chelating O,N,O environment to Cu^{II} (formation of two 5-membered chelating rings), while each of the deprotonated alkoxide O atoms can further bridge a Ln^{III} centre (Scheme 1). Following on our previous efforts, which led to $\{Cu^{II}_{15}Ln^{III}_7\}$ and $\{Cu^{II}_4Ln^{III}_8\}$ clusters with the pdm^{2-}/RCO_2^- ligation, we report here the synthesis and study of $\{Cu^{II}_5Ln^{III}_4\}$ complexes (Ln = Tb, Dy, Ho) along with their $\{Cu^{II}_5Y^{III}_4\}$ analogue.

Results and discussion

Synthetic comments and IR characterization

Most of the to-date reported 3d/4f-metal complexes containing the doubly (pdm^{2-}) or singly ($Hpdm^-$) form of H_2pdm as ligand are Cu^{II}/Ln^{III} clusters.[51,52,63,64] A common feature of all such complexes is that they possess a secondary (ancillary) carboxylate ligand. The general $Cu^{II}/Ln^{III}/H_2pdm/RCO_2^-$ reaction system is very fertile, and the identity of products has been found to depend on a number of synthetic parameters, the most important of which is the nature of R. Using rather similar reaction conditions (MeOH, MeOH/MeCN or MeOH/CH_2Cl_2 as solvent, Et_3N as base, RCO_2^- : H_2pdm reaction ratios

Open Access Article. Published on 25 November 2020. Downloaded on 2/21/2026 10:56:33 AM.
This article is licensed under a Creative Commons Attribution-NonCommercial 3.0 Unported Licence.

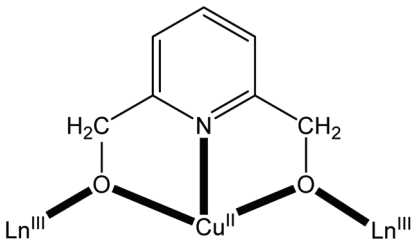

Scheme 1 The anticipated coordination mode of the doubly deprotonated pyridine-2,6-dimethanol (pdm^{2-}) ligand in Cu^{II}/Ln^{III} clusters.

equal to or higher than 1), our[51,52] and other[63,64] groups have isolated and studied four families of clusters. When R = Bu^t (*i.e.* the pivalate ion), the nonanuclear $[Cu_3Gd_6(OH)(CO_3)_4(O_2CBu^t)_9(pdm)_3(MeOH)_3]$[64] and $[Cu_8Gd_4(OH)_8(O_2CBu^t)_8(Hpdm)_8](ClO_4)_4$[63] complexes were prepared; for the isolation of the former, CO_2 gas was bubbled through the reaction solution. For R = Ph, the cage-like clusters $[Cu_{15}Ln_7(OH)_6(CO_3)_4(O_2CPh)_{19}(pdm)_9(H_2pdm)_3(H_2O)_2]$ (Ln = Gd, Dy) were obtained;[51] the CO_3^{2-} ions were derived from the fixation of atmospheric CO_2 under the basic conditions. In an attempt to further investigate this general reaction system, we used the *tert*-butylacetate ($Bu^tCH_2CO_2^-$) ion which had not been previously employed in 3d/4f-metal cluster chemistry; the result[52] was the isolation of members of the $[Cu_4Ln_8(OH)_6(NO_3)_2(O_2CCH_2Bu^t)_{16}(pdm)_4]$ (Ln = La, Gd, Tb, Dy) family of dodecanuclear clusters.

In the above mentioned families of clusters that contain the doubly deprotonated pdm^{2-} ligand, the $RCO_2^-:pdm^{2-}$ ratio in the formulae of the complexes is higher than 2, *i.e.* 3 in the $\{Cu_3Gd_6\}$ complex, 4 in the $\{Cu_4Ln_8\}$ family and ~2 in the $\{Cu_{15}Ln_7\}$ clusters. We suspected that clusters with more pdm^{2-} than RCO_2^- groups might be capable of existence and we set out experiments to prepare such products. Below we describe the realisation of this goal which provided access to a family of $\{Cu_5Ln_4\}$ clusters (Ln = Tb, Dy, Ho) containing an 1 : 2 $RCO_2^-:pdm^{2-}$ ratio.

The reaction of $Dy(NO_3)_3{\cdot}5H_2O$, $Cu(ClO_4)_2{\cdot}6H_2O$, H_2pdm, $Bu^tCH_2CO_2H$ and Et_3N in a 2 : 2.5 : 2 : 1 : 9 molar ratio in MeCN/MeOH led to a blue solution that upon storage at room temperature gave blue crystals of $[Cu_5Dy_4O_2(OMe)_4(NO_3)_4(O_2CCH_2Bu^t)_2(pdm)_4(MeOH)_2]{\cdot}4MeCN{\cdot}1.5MeOH$ (**1**·4MeCN·1.5MeOH) in ~35% yield. The crystals were of X-ray quality and the structure of the cluster was solved by single-crystal X-ray crystallography. A point of interest is that the nature of the copper(II) source does not affect the product identity; employment of $CuCl_2{\cdot}2H_2O$ or $Cu(NO_3)_2{\cdot}3H_2O$ gives again complex **1** in comparable yields, as evidenced by microanalyses and IR spectra. Completely analogous reactions with $Tb(NO_3)_3{\cdot}6H_2O$ and $Ho(NO_3)_3{\cdot}5H_2O$, using chloride or nitrate or perchlorate copper(II) sources, led to crystals of the isomorphous complexes $[Cu_5Tb_4O_2(OMe)_4(NO_3)_4(O_2CCH_2Bu^t)_2(pdm)_4(MeOH)_2]{\cdot}4MeCN{\cdot}1.5MeOH$ (**2**·4MeCN·1.5MeOH) and $[Cu_5Ho_4O_2(OMe)_4(NO_3)_4(O_2CCH_2Bu^t)_2(pdm)_4(MeOH)_2]{\cdot}4MeCN{\cdot}1.5MeOH$ (**3**·4MeCN·1.5MeOH), respectively. The isomorphous character of the three complexes was confirmed by determining the unit cell dimensions for the $\{Cu_5Tb_4\}$ and $\{Cu_5Ho_4\}$ clusters (*vide infra*).

Yttrium has radii (atomic, metallic, ionic) that fall close to those of Er and Ho, and all of its chemistry is in the trivalent state.[65] Hence it resembles the late lanthanides closely in its chemistry and occurs with them in nature. In the older literature in particular, it is not uncommon to find explicitly or implicitly the belief that an Y(III) complex of a given set of ligands will be isostructural with the corresponding late Ln(III) compounds. The test of this belief has been carried out for only a few complexes.[66–68] Somewhat to our surprise, use of $Y(NO_3)_3{\cdot}6H_2O$ instead of $Ln(NO_3)_3{\cdot}xH_2O$ (Ln = Tb, Dy, Ho) in an otherwise identical reaction system, gave complex $[Cu_5Y_4O_2(OMe)_4(NO_3)_2(O_2CCH_2Bu^t)_4(pdm)_4(MeOH)_2]{\cdot}2MeOH$ (**4**·2MeOH) which contains two nitrato (instead of four in **1–3**) and four *tert*-butylacetato (instead of two in **1–3**) ligands.

Description of structures

The structures of **1**·4MeCN·1.5MeOH and **4**·2MeOH were solved by single-crystal X-ray crystallography. Compound **1**·4MeCN·1.5MeOH crystallizes in the monoclinic space group *I*2/*m* (Table S1†) with the asymmetric unit containing $\frac{1}{4}$ of the cluster $[CuCu_4{*}Dy_4O_2(OMe)_4(NO_3)_4(O_2CCH_2Bu^t)_2(pdm)_4(MeOH)_2]$ (Fig. 1 and S1†); the star (*) on the second Cu^{II} atom indicates that this cation occupies a site with different symmetry from the unstarred one. The point group symmetry is 2/*m* (C_{2h}). The nonanuclear cluster molecule contains five Cu^{II} and four Dy^{III} atoms. The core of the cluster, shown in Fig. 2, is $\{Cu_5Dy_4(\mu_5\text{-}O)_2(\mu_3\text{-}O_{MeO}^-)_4(\mu\text{-}O_{MeOH})_2(\mu\text{-}OR')_8\}^{6+}$, where R′ is the carbon/nitrogen/hydrogen containing part of pdm^{2-}.

Concerning the symmetry elements, the central Cu^{II} atom (Cu2) lies on 2/*m* site symmetry. The mirror plane possessed by

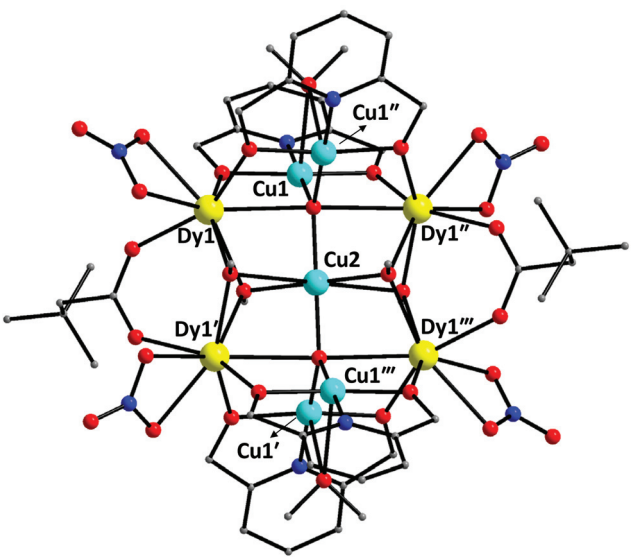

Fig. 1 The structure of the cluster molecule $[Cu_5Dy_4O_2(OMe)_4(NO_3)_4(O_2CCH_2Bu^t)_2(pdm)_4(MeOH)_2]$ that is present in the crystal of **1**·4MeCN·1.5MeOH. Symmetry codes: (′) *x*, 1 − *y*, *z*; (″) 2 − *x*, *y*, −*z*; (‴) 2 − *x*, 1 − *y*, −*z*.

This journal is © The Royal Society of Chemistry 2021

Open Access Article. Published on 25 November 2020. Downloaded on 2/21/2026 10:56:33 AM.
This article is licensed under a Creative Commons Attribution-NonCommercial 3.0 Unported Licence.

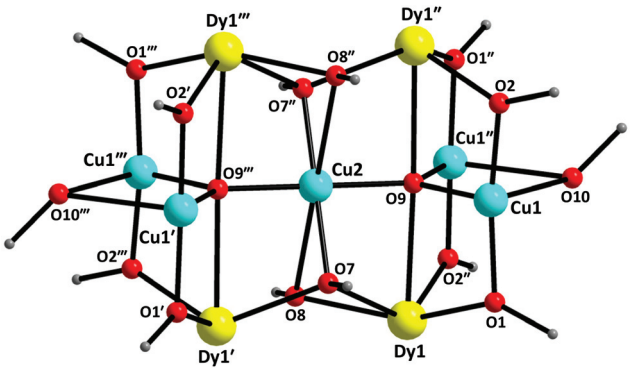

Fig. 2 The $\{Cu_5Dy_4(\mu_5\text{-}O)_2(\mu_3\text{-}O_{MeO}^-)_4(\mu\text{-}O_{MeOH})_2(\mu\text{-}OR')_8\}^{6+}$ core of the cluster molecule **1**. O9, O9‴ represent the μ_5-oxo groups; O7, O7″, O8, O8″ are the μ_3-methoxo oxygen atoms; O10, O10‴ denote the bridging methanol oxygen atoms; O1, O2 and their symmetry equivalents belong to the pdm^{2-} ligands. The symmetry codes are the same with those defined in the caption of Fig. 1.

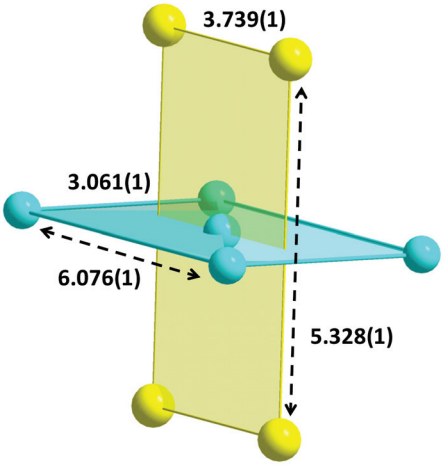

Fig. 3 The metallic skeleton in **1**·4MeCN·1.5MeOH; the numbers indicate distances in Å. Colour code: Cu^{II}, cyan; Dy^{III}, yellow.

the molecule is defined by Cu2, the four backbone carbon atoms (and their symmetric ones) that belong to the $Bu^tCH_2CO_2^-$ ligands, and the four carbon and oxygen atoms of the methoxo groups (and their symmetry equivalents). The two-fold axis is defined by Cu2 and the two μ_5-O^{2-} atoms (O9, O9‴).

The five Cu^{II} atoms are co-planar forming a bow-tie arrangement. The four outer Cu^{II} atoms (Cu1, Cu1′, Cu1″, Cu1‴) form a rectangle with edges of 3.061(1) and 6.076(1) Å; the central-to-outer Cu2–Cu(1,1′,1″,1‴) distance is 3.402(1) Å. The four Dy^{III} atoms also form a rectangle (Fig. 3) that lies above and below the plane of the Cu^{II} centres, with edges of 3.739(1) and 5.328(1) Å; the diagonal of this rectangle is 6.509(1) Å. The two, strictly planar rectangles are almost perpendicular forming an angle of 89.0(1)°. The Cu···Dy distances between the outer Cu^{II} atoms and the Dy^{III} centres are in the range 3.266(1)–5.778(1) Å, whereas the distance of the central Cu^{II} atom to the Dy^{III} centres is 3.255(1) Å. Overall the metallic skeleton can be described as four face- and vertex-sharing $\{Cu_3Dy\}$ tetrahedral units.

Two trigonal bipyramidal μ_5-O^{2-} groups (O9 and O9‴) link the perpendicular Cu_5 and Dy_4 frameworks together. Each of them bridges the central Cu2 atom with two Cu^{II} centres of the short edge of the Cu_4 rectangle and with two Dy^{III} centres that belong to a long edge of the Dy_4 rectangle. The four methoxo groups (defined by O7, O8, O7″ and O8″) display a μ_3 mode each bridging the central Cu2 atom with two Dy^{III} atoms of the short edge of the Dy_4 rectangle. The oxygen atoms (O10, O10‴) of the neutral MeOH molecules bridge two Cu^{II} atoms that belong to a short edge of the Cu_4 rectangle; these atoms lie on a two-fold axis of symmetry and each MeOH molecule is thus disordered over two positions. The two $Bu^tCH_2CO_2^-$ groups (equivalent by symmetry) behave as *syn*,*syn* η^1:η^1:μ ligands, each bridging two Dy^{III} atoms that belong to a short edge of the Dy_4 rectangle. The four η^2:η^1:η^2:μ_3 pdm^{2-} ligands each chelate one of the four outer Cu^{II} atoms forming two 5-membered chelating rings and simultaneously bridge two Dy^{III} centres of the long edge of the Dy_4 rectangle. The four terminal nitrato groups each chelate (η^1:η^1) one of the four Dy^{III} atoms. The coordination modes of the ligands that are present in **1**·4MeCN·1.5MeOH are summarized in Fig. 4.

The central Cu^{II} atom, Cu2, is 6-coordinate and presents a Jahn–Teller elongated (4 + 2) tetragonal bipyramidal geometry with a $\{Cu^{II}O_6\}$ coordination sphere. The long Cu2–O8 (and its symmetry equivalent) distance of 2.746(6) Å can be considered as a weak interaction. The four bonds in the equatorial plane are much shorter [1.922(4) and 1.985(4) Å]. The outer copper(II) (Cu1 and its symmetry equivalents) coordination geometries are described as distorted square pyramidal with the bridging MeOH oxygen atom (O10) occupying the apical position. The coordination sphere is of the $\{Cu^{II}O_4N\}$ type. Analysis of the shape-determining angles using the approach of Reedijk and Addison[69] yields a value of 0.19 for the trigonality index τ (τ = 0 and 1 for perfect square pyramidal and trigonal bipyramidal geometries, respectively). As expected, the axial bond [Cu1–O10 = 2.515(4) Å] is the longest, the coordination bond lengths in the basal plane being in the 1.879(4)–1.951(3) Å range. The crystallographically unique Dy^{III} centre is 8-coordinate

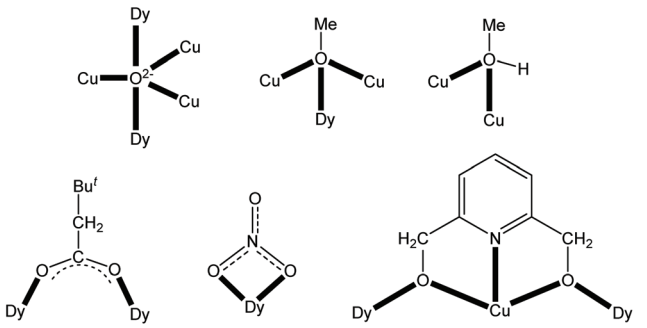

Fig. 4 The coordination modes of all the ligands that are present in **1**·4MeCN·1.5MeOH; the coordination bonds are indicated with bold lines.

Open Access Article. Published on 25 November 2020. Downloaded on 2/21/2026 10:56:33 AM.
This article is licensed under a Creative Commons Attribution-NonCommercial 3.0 Unported Licence.

with a $\{Dy^{III}O_8\}$ coordination sphere and Dy–O distances in the 2.241(3)–2.664(1) Å range. To estimate the closer coordination polyhedron defined by the eight donor atoms around the Dy^{III} centre in **1**·4MeCN·1.5MeOH, a comparison of the experimental data with the theoretical values for the most common polyhedral shapes with 8 vertices was performed using the SHAPE program.[70] The best fit was obtained for the Snub diphenoid JSD – 8 (CShM = 2.744), Fig. S2† (left). Since the nitrato group imposes a small bite angle, the polyhedron is distorted.

The molecules in the crystal of **1**·4MeCN·1.5MeOH interact through non-classical hydrogen bonds and they are arranged in a body-centered lattice in conformity with the *I*2/*m* space group, forming channels along the *a* and *c* crystallographic axes where the lattice MeCN and MeOH molecules are residing (Fig. S3†).

The crystal structure of **4**·2MeOH consists of cluster molecules $[Cu_5Y_4O_2(OMe)_4(NO_3)_2(O_2CCH_2Bu^t)_4(pdm)_4(MeOH)_2]$ (Fig. 5 and S4†) and lattice MeOH molecules in a 1 : 2 ratio; the latter will not be further discussed. The complex crystallizes in the triclinic space group $P\bar{1}$ with the asymmetric unit containing half the cluster, which lies upon an inversion centre. The structure of the molecule **4** is very similar with that of **1**. Again the core is $\{Cu_5Y_4(\mu_5\text{-}O)_2(\mu_3\text{-}O_{MeO}^-)_4(\mu\text{-}O_{MeOH})_2(\mu\text{-}OR')_8\}^{6+}$ (Fig. S5†). Notable differences (except the presence of four Y^{III} centres instead of four Dy^{III} atoms) are: (i) **1** possesses 2/*m* point group symmetry while **4** is centrosymmetric; (ii) two of the chelating nitrato groups of **1** have been replaced by two chelating $Bu^tCH_2CO_2^-$ ligands in **4** and the composition of the two cluster molecules is thus different; and (iii) the coordination polyhedra of the two crystallographically independent Y^{III} atoms (Y1 and Y2) in **4** can be described as biaugmented trigonal prisms (CShM = 2.825 for Y1 and 2.271 for Y2), whereas the polyhedron of the crystallographically unique Dy^{III} centre in **1** is Snub diphenoid (Fig. S2†).

The edges of the Cu_4 rectangle consisting of the four outer Cu^{II} atoms are 3.124(1) Å (Cu1···Cu2 = Cu1′···Cu2′) and 5.978 (1) Å (Cu1···Cu2′ = Cu2···Cu1′), where prime (′) is the symmetry operation $2 - x$, $2 - y$, $2 - z$. The edges of the Y_4 rectangle are 3.766(1) Å (Y1···Y2 = Y1′···Y2′) and 5.419(1) Å (Y1···Y2′ = Y2···Y1′). The two rectangles are strictly planar by symmetry; the two planes are almost perpendicular with a dihedral angle of 89.3(1)°. As in **1**, the central Cu^{II} atom (Cu2) is 6-coordinate with a $\{Cu^{II}O_6\}$ coordination sphere and an elongated (4 + 2) tetragonal bipyramidal geometry. Two of its six coordination bonds are considered as long contacts [Cu3–O14 = Cu3–O14′ = 2.785(3) Å], whereas the four equatorial bonds are much shorter [Cu3–O13 = Cu3–O13′ = 1.992(2) Å and Cu3–O15 = Cu3–O15′ = 1.919(2) Å]. The coordination geometries of the outer Cu^{II} atoms are square pyramidal (τ = 0.08 for Cu1, Cu1′ and 0.04 for Cu2, Cu2′), with the bridging MeOH oxygen atom (O12 and its symmetry equivalent) occupying the apical position. As expected, the Cu1–O12 and Cu2–O12 bonds are long [Cu1–O12 = 2.563(3) Å, Cu2–O12 = 2.495(2) Å], whereas the corresponding bond distances in the basal planes lie in the range 1.884(2)–1.950(2) Å. The coordination spheres of the Y^{III} atoms are of the $\{Y^{III}O_8\}$ type, with bond distances in the 2.243 (2)–2.527(2) Å range.

The molecules in the crystal of **4**·2MeOH interact through hydrogen bonds and form layers parallel to the (001) crystallographic plane (Fig. S6†). Molecules belonging to neighbouring layers further interact through van der Waals forces and are stacked along the *c* crystallographic axis, thus building the 3D architecture of the structure.

Complexes **1–3** are new members of the small family of 3d/4f-metal clusters containing H_2pdm and its anionic forms as ligands.[51,52,60–64] The previously characterized compounds are conveniently summarized in Table 1, together with diagnostic structural and magnetic information. It is clear that the nuclearity, metallic skeleton and core are all unique in the clusters of the present work. As far as the $H_2pdm/Hpdm^-/pdm^{2-}$: RCO_2^- ratio is concerned, compounds **1–3** contain the highest ratio by far and this has a variety of structural consequences.

Compounds **1–4** also join a small group of $\{M^x_5Ln_4\}$ and $\{M^x_5Y_4\}$ clusters, where M is a 3d-metal and x = II–IV. The previously characterized complexes are listed in Table 2, together with their metal topology and magnetic characteristics. With the exception of the members of the $[Cu^{II}_5Ln_4O_2(OMe)_4(NO_3)_4(O_2CBu^t)_2(Htea)_4]$ (Ln = Gd, Tb, Dy, Ho) family ($Htea^{2-}$ is the dianion of triethanolamine),[73–75] complexes **1–3** have a different composition and different structural features compared with those of the previously characterized complexes. The molecular structure of **1** is quite similar to the structure of the $\{Cu^{II}_5Ln_4\}/Htea^{2-}$ clusters. The $Htea^{2-}$ groups adopt the $\eta^2{:}\eta^1{:}\eta^2{:}\mu_3$ coordination mode exhibited by the pdm^{2-} ligand in **1** (Fig. 4). The coordination modes of the oxide, methoxide, nitrate and carboxylate ligands are exactly the same. The metallic skeletons are also very similar. These experimental observations, emphasized in Fig. S7,† indicate that the pdm^{2-} *vs.* $Htea^{2-}$ and $Bu^tCH_2CO_2^-$ *vs.* $Bu^tCO_2^-$ changes have little structural effect (this structural similarity is extended to **4**, despite its slightly different chemical composition). However, there are three differences between the molecular structures of **1** and $[Cu^{II}_5Ln_4O_2(OMe)_4(NO_3)_4(O_2CBu^t)_2(Htea)_4]$: (i) the μ-MeOH group is missing in the $Htea^{2-}$ clusters resulting in a

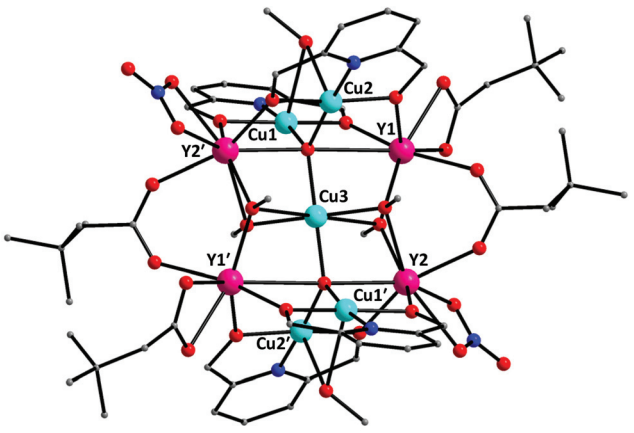

Fig. 5 The structure of the cluster molecule $[Cu_5Y_4O_2(OMe)_4(NO_3)_2(O_2CCH_2Bu^t)_4(pdm)_4(MeOH)_2]$ that is present in the crystal of **4**·2MeOH. Symmetry code: (′) $2 - x$, $2 - y$, $2 - z$.

This journal is © The Royal Society of Chemistry 2021

Open Access Article. Published on 25 November 2020. Downloaded on 2/21/2026 10:56:33 AM.
This article is licensed under a Creative Commons Attribution-NonCommercial 3.0 Unported Licence.

Table 1 To-date characterized heterometallic 3d/4f-metal complexes of $Hpdm^-$ and pdm^{2-}, and diagnostic information

Complex[a]	Coordination mode of $Hpdm^-$ and pdm^{2-}	Metal topology	Magnetic features	Ref.
$[Co^{II}_2Ln_2(O_2CBu^t)_4(Hpdm)_4]$ (Ln = Y, Gd, Tb, Dy, Ho)	$\eta^3{:}\eta^1{:}\mu_3$	Cubane	SMM (Ln = Dy)	61
$[Mn^{II}Mn^{III}Ln_2(O_2CMe)_6(L)(Hpdm)_2](NO_3)$[b] (Ln = Gd, Dy)	$\eta^2{:}\eta^1{:}\eta^1{:}\mu$	Butterfly	Weak F exchange	62
$[Fe^{III}_2Ln_2Cl_4(Hpdm)_6]Cl_2$ (Ln = Y, Ho)	$\eta^2{:}\eta^1{:}\eta^1{:}\mu$, $\eta^2{:}\eta^1{:}\mu$	U-shaped	AF exchange	60
$[Cu^{II}_4Ln_8(OH)_6(NO_3)_2(O_2CCH_2Bu^t)_{16}(pdm)_4]$ (Ln = La, Gd, Tb, Dy)	$\eta^3{:}\eta^1{:}\eta^1{:}\mu_3$, $\eta^2{:}\eta^1{:}\eta^2{:}\mu_3$	Cage-like	SMM (Ln = Dy)	52
$[Cu^{II}_{15}Ln_7(OH)_6(CO_3)_4(O_2CPh)_{19}(pdm)_3(H_2pdm)_9(H_2O)_2]$[c] (Ln = Gd, Dy)	$\eta^3{:}\eta^1{:}\eta^2{:}\mu_4$	Cage-like	Magnetic refrigerant (Ln = Gd), SMM (Ln = Dy)	51 and 71
$[Cu^{II}_3Gd_6(OH)(CO_3)_4(O_2CBu^t)_9(pdm)_3(MeOH)_3]$	$\eta^2{:}\eta^1{:}\eta^2{:}\mu_3$	Tridiminished icosahedron	Magnetic refrigerant	64
$[Cu^{II}_8Gd_4(OH)_8(O_2CBu^t)_8(Hpdm)_8](ClO_4)_4$	$\eta^3{:}\eta^1{:}\mu_3$	Wheel of four corner-sharing $\{Cu^{II}_2Gd_2\}$ cubanes	[d]	63

[a] Lattice solvent molecules have been omitted. [b] L is the dianionic ligand (6-hydroxymethylpyridin-2-yl)(6-hydroxymethylpyridin-2-ylmethoxy) methanol obtained from the *in situ* reaction of two H_2pdm groups. [c] The neutral H_2pdm molecules behave as $\eta^2{:}\eta^1{:}\eta^1{:}\mu$ ligands. [d] Information was not provided. F = ferromagnetic; AF = antiferromagnetic.

Table 2 To-date characterized $\{M_5Ln_4\}$ complexes and diagnostic information (M = 3d-metal ion)

Complex[a]	Metal topology	Magnetic features	Ref.
$[Mn^{III}_4Mn^{IV}Ln_4O_6(NO_3)_4(O_2CBu^t)_6(mdea)_2(Hmdea)_2(H_2O)_2]$[b] (Ln = Y, Tb, Dy, Ho)	Two $\{Mn^{IV}Mn^{III}Ln_2\}$ cubanes sharing a Mn^{IV} vertex	SMMs (all)	72
$[Cu^{II}_5Ln_4O_2(OMe)_4(NO_3)_4(O_2CBu^t)_2(Htea)_4]$[c] (Ln = Gd, Tb, Dy, Ho)	Four face- and vertex-sharing tetrahedral units	Magnetic refrigerant (Ln = Gd) SMMs (Ln = Tb, Dy, Ho)	73–75
$[Cu^{II}_5Dy_4(OH)_4(SCN)_8(H_2L)_4]Cl_2$ [d]	[3 × 3]-shaped heterometallic grid	SMM	76
$[Fe^{III}_5Gd_4O_4(NO_3)_2$(bis-C[4])$_2(DMF)_8(H_2O)_2](OH)$[e]	Two $\{Fe^{III}_2Gd_2\}$ butterflies linked by a central Fe^{III} cation	Competing F–AF exchange interactions	77
$[M^{II}_5Ln_4(OMe)_8(NO_3)_2(O_2CMe)_{12}(MeOH)_6]$ (M/Ln = Co/Eu, Co/Gd, Ni/Eu, Ni/Dy)	Two $\{M^{II}_2Ln_2\}$ cubanes connected *via* a M^{II} centre	Magnetic refrigerant ($\{Co^{II}_5Gd_4\}$) SMMs ($\{Co^{II}_5Eu_4\}$ and $\{Ni^{II}_5Dy_4\}$)	78
$[M^{II}_5Ln_4(OH)_2(OMe)_6(NO_3)_4(O_2CMe)_{10}(MeOH)_6]$ (M/Ln = Co/Dy, Ni/Gd)	Two $\{M^{II}_2Ln_2\}$ cubanes connected *via* a M^{II} centre	Magnetic refrigerant ($\{Ni^{II}_5Gd_4\}$) SMM ($\{Co^{II}_5Dy_4\}$)	78

[a] Lattice solvent molecules have been omitted. [b] The ligands mdea and Hmdea are the di- and monoanions of *N*-methyl-diethanolamine. [c] The ligand Htea is the dianion of triethanolamine. [d] H_2L is the dianionic form of a polydentate ligand synthesised by the reaction of pyridine-2,6-dicarbohydrazide and two equiv. of 6-hydroxymethylpyridine-2-carbaldehyde. [e] The ligand bis-C[4] is the octaanion of bis-Bu^t-calix[4]arene. F = ferromagnetic; AF = antiferromagnetic.

square planar coordination for the outer Cu^{II} atoms and a longer distance (~3.29 *vs.* ~3.06 Å) between the Cu^{II} centres that occupy the short edges of the Cu_4 rectangle; (ii) the coordination polyhedron in **1** approximates a Snub diphenoid, whereas that in the $Htea^{2-}$ clusters is best described as a square antiprism; and (iii) **1** possesses 2/*m* symmetry, while the $Htea^{2-}$ clusters are simply centrosymmetric with respect to the central Cu^{II} atom, *i.e.* that in the middle of the rectangle.

Magnetic studies

Direct current (dc) magnetic susceptibility (χ_M) data on well-dried and analytically pure samples of **1–3** were collected in the 300–2 K temperature range under fields of 0.3 T (300–30 K) and 0.02 T (30–2 K). The data are plotted as $\chi_M T$ products *vs.* *T* in Fig. 6. Compounds **1–3** have room-temperature $\chi_M T$ values of 58.5, 48.7 and 57.1 cm^3 K mol^{-1}, respectively. These values are in good agreement with those expected for five Cu^{II} atoms (S = 1/2, g = 2) and four Dy^{III} atoms (S = 5/2, L = 5, $^6H_{15/2}$, g_J = 4/3) [the theoretical value is 58.55 cm^3 K mol^{-1}] for **1**, for five Cu^{II} atoms (S = 1/2, g = 2) and four Tb^{III} atoms (S = 3, L = 6, $^7F_6$, g_J = 3/2) [the theoretical value is 49.11 cm^3 K mol^{-1}] for **2**, and for five Cu^{II} atoms (S = 1/2, g = 2) and four Ho^{III} atoms (S = 2, L = 6, g_J = 5/4) [the theoretical value is 57.78 cm^3 K mol^{-1}] for **3**, with the assumption that there are no interactions between the spin carriers. Upon cooling, the $\chi_M T$ value of **1** decreases slowly to 54.05 cm^3 K mol^{-1} at 26 K, to 42.43 cm^3 K mol^{-1} at 12 K for **2** and to 51.81 cm^3 K mol^{-1} at 20 K for **3**. Below these temperatures, the $\chi_M T$ values increase abruptly reaching the values of 85.35 (**1**), 55.69 (**2**) and 70.65 cm^3 K mol^{-1} (**3**) at 2 K. The slight decrease is due to the depopulation of the m_j sublevels of the ground J state of the Ln^{III} centres (Stark sublevels) and may also be due to weak antiferromagnetic interactions between the metal ions. The large increase in $\chi_M T$ values at low temperatures suggests ferromagnetic interactions, with large spin ground states for the complexes. Magnetization (*M*) *vs.* external applied field (*H*) studies at 2 K (inset of Fig. 6) show a rapid increase of *M* as *H* increases reaching almost saturation values of 23.20, 21.17 and 22.65 Nμ_B for **1**, **2** and **3**, respectively, at 5 T and 2 K, suggesting large spin ground states.

Open Access Article. Published on 25 November 2020. Downloaded on 2/21/2026 10:56:33 AM.
This article is licensed under a Creative Commons Attribution-NonCommercial 3.0 Unported Licence.

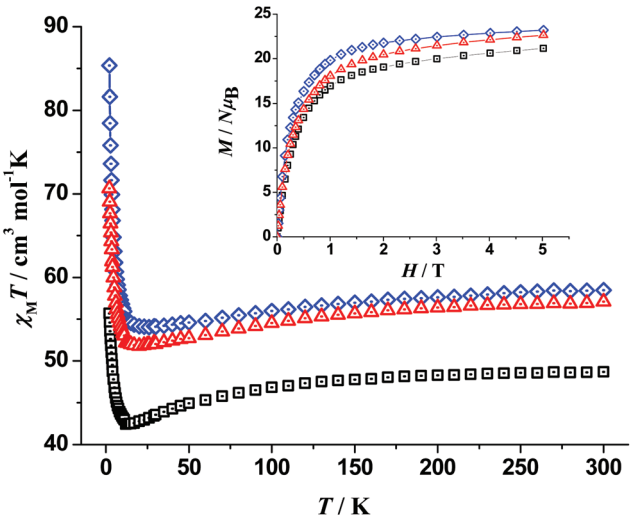

Fig. 6 Temperature dependence of the $\chi_M T$ product for complexes **1** (blue diamonds), **2** (black squares) and **3** (red triangles); the field dependence of the magnetization at 2 K is shown in the inset. The lines are guides to the eye.

The value of the $\chi_M T$ product for **4** at 300 K is 1.50 cm^3 K mol^{-1}, lower than the theoretical value of 1.875 cm^3 K mol^{-1} expected for five non-interacting Cu^{II} (S = 1/2, g = 2) centres. Upon cooling, the value of the product decreases rather slowly reaching ~1.2 cm^3 K mol^{-1} at ~50 K and then decreases rapidly to the value of 0.84 cm^3 K mol^{-1} at 2 K (Fig. 7). M increases rapidly as H increases at 2 K to the value of ~2 Nμ_B at 5 T without reaching saturation. The diamagnetic character of Y^{III} allowed us to fit the experimental data of the static magnetic properties taking into account only the five Cu^{II} atoms which are arranged as two vertex-sharing triangles; the Cu^{II} atoms of each triangle are bridged by a μ_3-O^{2-} group (the oxo groups are structurally μ_5, Fig. S5†) resulting in two superexchange pathways, as shown in the inset of Fig. 7.

Using the program PHI,[79] the data were fitted using the spin Hamiltonian given by eqn (1). The best-fit parameters in the 300–35 K range are J_1 = −102(1) cm^{-1}, J_2 = −58(1) cm^{-1} and g = 2.24. Taking into account the large Cu–O–Cu angles [Cu1–O15–Cu2 = 110.8(1)°, Cu1–O15–Cu3 = 123.7(1)° and Cu2–O15–Cu3 = 124.6(1)°; see Fig. S5†], moderately strong antiferromagnetic Cu^{II}···Cu^{II} exchange interaction with $|J_1| > |J_2|$ should be expected. From the inset of Fig. 7, it is clear that the ground state will be S = 3/2 if J_1 dominates, whereas the ground state will be S = 1/2 if the dominating interaction is J_2. Intermediate low-temperature $\chi_M T$ or magnetization values could be found around the frustration point $J_1 = 2J_2$; this seems to be the case here.

$$H = -2J_1(S_1 \cdot S_2 + S_1 \cdot S_3 + S_1 \cdot S_4 + S_1 \cdot S_5) - 2J_2(S_2 \cdot S_3 + S_4 \cdot S_5) \quad (1)$$

The dynamic magnetic properties of **1–3** were investigated in search of slow relaxation in the magnetization response (SMM behaviour). Preliminary measurements at the fixed, alternating current (ac) frequency of 1000 Hz and variable field revealed clear temperature dependence of the imaginary, out-of-phase component of the ac susceptibility, χ''_M, at zero field for **1**, weak tails at zero field with increasing intensity up to 0.2 T of transverse field for **2** and poorly field-dependent tails for **3**. According to this preliminary information, ac measurements were performed at zero dc field for **1** and **3**, and under an applied field of 0.2 T for **2** (Fig. 8).

The temperature dependence of χ''_M for **1** in the 10–1488 Hz range at zero field is shown in the left part of Fig. 8; signals appear above 2 K. The value of the relaxation time τ ($\tau = 1/2\pi\nu$) is large (7.6×10^{-3} s) at 2.1 K. The data were fitted using an Arrhenius model, $\tau = \tau_0 \exp(U_{eff}/k_B T)$, by using two different methods: the data from the χ''_M *vs.* T plot, and the data from the χ''_M *vs.* frequency (ν) plot, assuming a magnetization relaxation through an Orbach process. Comparable relaxation parameters were obtained. The fit of the higher-temperature

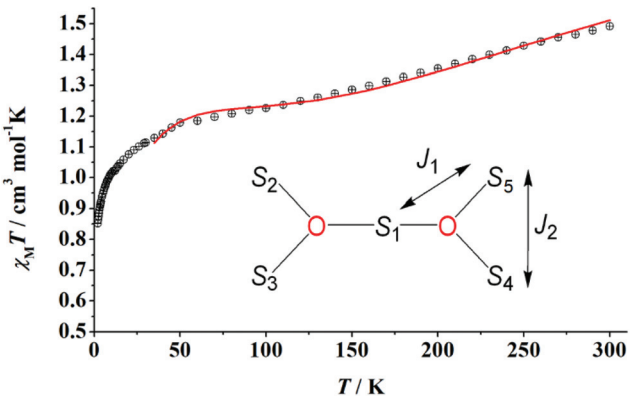

Fig. 7 $\chi_M T$ *vs.* T plot for **4**; the red solid line is the best-fit curve (see text for details). The coupling scheme for the molecule is shown in the inset with the $S_{i\ (i=1-5)}$ spin carriers representing the five Cu^{II} atoms; S_1 is Cu3 of the real structure.

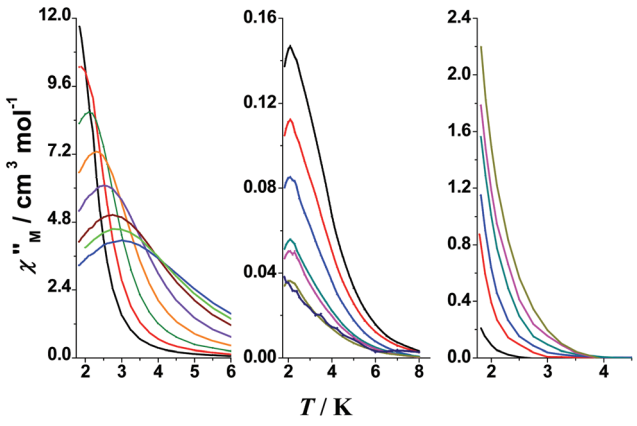

Fig. 8 (Left) χ''_M *vs.* T signals for **1** in the 10–1488 Hz range at zero field; (middle) χ''_M *vs.* T signals for **2** in the 1.45–148 Hz range under an applied dc field of 0.2 T; (right) χ''_M *vs.* T signals for **3** in the 10–1488 Hz range at zero field. Solid lines are visual guides.

This journal is © The Royal Society of Chemistry 2021

Open Access Article. Published on 25 November 2020. Downloaded on 2/21/2026 10:56:33 AM.
This article is licensed under a Creative Commons Attribution-NonCommercial 3.0 Unported Licence.

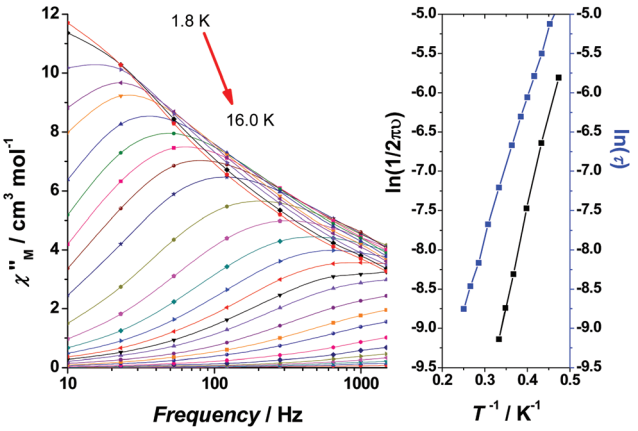

Fig. 9 (Left) χ''_M *vs.* ν plot for **1** at zero dc field in the indicated temperature range (solid lines are guides for the eye); (right) Arrhenius plots of ln(1/2πν) (left line) and ln(τ) *vs.* T^{-1} for **1** (the solid lines represent the fits that give the U_{eff} and τ_0 values mentioned in the text).

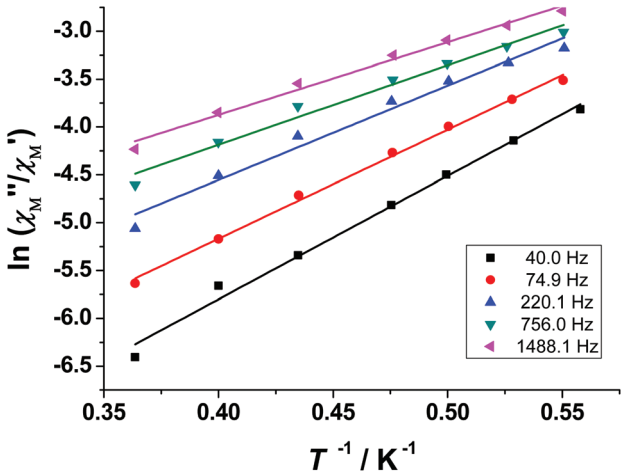

Fig. 10 Plots of ln(χ''_M/χ'_M) *vs.* 1/T for **3** (the temperature range is 1.8–2.75 K) at different ac frequencies; the solid lines are the best-fit curves.

maxima in the χ''_M *vs.* T plot yields U_{eff} = 16.7 cm^{-1} (~24 K) and $\tau_0 = 3.75 \times 10^{-8}$ s, while the fit of τ from the χ''_M *vs.* ν plot for a wider temperature range yields U_{eff} = 12.2 cm^{-1} (17.6 K) and $\tau_0 = 2.0 \times 10^{-6}$ s, Fig. 9. The linear dependence of ln(τ) with the inverse temperature suggests the occurrence of only one relaxation process, in agreement with the Argand plot (Fig. S8†) in which only one semicircle appears.

Measurements of the dynamic magnetic properties of **2** exhibited very weak out-of-phase susceptibility signals under an applied field of 0.2 T, which are poorly field-dependent and decrease for higher frequencies, Fig. 8 (middle). Maxima with negligible frequency dependence were defined for low frequencies (1.45–10 Hz). This behaviour of the ac curves indicates magnetic relaxation through a tunneling mechanism.

The magnetization dynamics of the $\{Cu^{II}_5Ho_4\}$ cluster **3** were investigated in the 10–1500 Hz frequency range. The χ''_M *vs.* T plots show only tails (Fig. 8, right), indicating that slow magnetization relaxation occurs below 2 K (the lowest-temperature limit of our setup). Because no maxima in χ''_M were observed, we were unable to determine the energy barrier U_{eff} and the pre-exponential factor τ_0 *via* the conventional Arrhenius plot method. Another method, established by Bartolomé *et al.*,[80] is to assume that there is only one characteristic relaxation process of the Debye type with one energy barrier and one time constant. From eqn (2) and by plotting ln(χ''_M/χ'_M) *vs.* 1/T, we can perform linear regressions to obtain the gradients (E_a/k_B) and intercepts [ln($\omega\tau_0$)] and then extract an estimation of the activation energy and τ_0; χ'_M is the real, in-phase component of the ac susceptibility and $\omega = 2\pi\nu$. These estimates for **3** are $U_{eff} \approx E_a$ = 10.0 ± 0.1 K and τ_0 = 7.1(± 0.2) × 10^{-7} s (Fig. 10).

$$\ln(\chi''_M/\chi'_M) = \ln(\omega\tau_0) + E_a/k_BT \quad (2)$$

A comparison of the magnetic properties of **1–3** with those of the structurally similar clusters $[Cu_5Ln_4O_2(OMe)_4(NO_3)_4(O_2CBu^t)_2(Htea)_4]$ (Ln = Dy, Tb, Ho)[74] might be useful at this point. The $Htea^{2-}$ clusters also have large spin ground states and exhibit slow relaxation of the magnetization, the $U_{eff} = E_a$ values estimated to be 7 ± 1 K, 11.9 ± 0.8 K and 10 ± 4 K for the Dy(III), Tb(III) and Ho(III) members, respectively. The values for the Ho(III) clusters seem to be comparable, while the U_{eff} value for **1** is higher (at least double) than that for the $Cu^{II}/Dy^{III}/Htea^{2-}$ cluster. *Ab initio* calculations that employ Dy^{III} and Cu^{II} fragments of $[Cu_5Dy_4O_2(OMe)_4(NO_3)_4(O_2CBu^t)_2(Htea)_4]$ and the lowest Kramers levels resulting therefrom yielded[74] good fits of the susceptibility *vs.* temperature behaviour and a corresponding set of best-fit J_1 ($Cu^{II}\cdots Dy^{III}$), J_2 (Cu^{II} central$\cdots Cu^{II}$ outer) and J_3 (Cu^{II} outer$\cdots Cu^{II}$ outer) values. The first two J values correspond to ferromagnetic pathways and the third corresponds to antiferromagnetic pathways. The exchange interaction between Dy^{III} ions is negligible due to the perpendicular arrangement of the main anisotropy axes. The main anisotropy axis of the cluster molecule is almost perpendicular to the plane defined by the four Dy^{III} centres.

Concluding comments and perspectives

Complexes **1–3** are the first members of a new, fifth family of clusters arising from the general $Cu^{II}/Ln^{III}/H_2pdm/RCO_2^-$ reaction system. By contrast with the previously reported $\{Cu_3Gd_6\}$,[64] $\{Cu_8Gd_4\}$,[63] $\{Cu_{15}Ln_7\}$[51] and $\{Cu_4Ln_8\}$[52] families which contain a RCO_2^- : primary ligand ratio higher than 2, in the $\{Cu_5Ln_4\}$ complexes of the present family this ratio is 0.5 leading to a different nuclearity, topology and core. The $\{Cu_5Ln_4\}$ clusters were prepared by simply using an excess of H_2pdm ($H_2pdm : RCO_2^-$ = 2 : 1) in the reaction mixtures. Thus, the chemical message of this work is that a detailed investigation of all synthetic parameters (here the primary to ancillary ligand reaction ratio) is more than necessary to isolate the

Open Access Article. Published on 25 November 2020. Downloaded on 2/21/2026 10:56:33 AM.
This article is licensed under a Creative Commons Attribution-NonCommercial 3.0 Unported Licence.

maximum number of 3d/4f-metal products from a given reaction system. From the magnetism viewpoint, complexes **1–3** exhibit different characteristics concerning their magnetization relaxation. The Dy^{III}-containing cluster **1** behaves as a SMM, which is the expected behaviour due to the high magnetic moment and Kramer's nature of Dy^{III}, that ensures the degeneracy of the two lowest-lying levels and reduces the possibility of the relaxation of the magnetization *via* quantum tunneling.[34] This is confirmed by examining the magnetic relaxation of the Tb^{III} and Ho^{III} analogues (**2** and **3**, respectively). Both are non-Kramers ions and strong tunneling is the principle magnetization relaxation making **2** a very weak field-induced SMM with ac maxima practically independent of the frequency, while **3** exhibits only weak tails in the χ''_M *vs.* *T* plots at zero dc field.

With the above results in mind, we continue working in the area of the chemistry and magnetism of Cu^{II}/Ln^{III} cluster chemistry using the H_2pdm/RCO_2^- ligand "blend", paying more attention to the study of the influence of R on the chemical and structural identity of the products. Although $Cu^{II}/Ln^{III}/pdm^{2-}$ or $Hpdm^-$ clusters with R = Ph,[51] Bu^t,[63,64] and Bu^tCH_2 [52] (together with results of the present work) have been reported, there is a plethora of R groups with various electronic and steric properties that can be examined. Ongoing studies reveal new families of $Cu^{II}/Ln^{III}/pdm^{2-}$ clusters with novel structures and interesting magnetic properties, proving that the general $Cu^{II}/Ln^{III}/H_2pdm/RCO_2^-$ reaction system is fertile and surprising. Our results, already well advanced, will be reported soon.

Experimental section

General, physical measurements and spectroscopic studies

All manipulations were performed under aerobic conditions using materials (reagent grade) and solvents as received. Elemental analyses were performed by the University of Patras microanalytical service. FT-IR spectra (4000–400 cm^{-1}) were recorded using a PerkinElmer spectrometer with samples prepared as KBr pellets. Direct-current (dc) and alternating-current (ac) magnetic susceptibility studies were performed at the University of Barcelona Chemistry Department on a DSM5 Quantum Design magnetometer operating at 0.3 T in the 300–30 K range and at 0.02 T in the 30–2.0 K range to avoid saturation effects. Pascal's constants were used to estimate the diamagnetic contribution, which was subtracted from the experimental susceptibility to give the molar paramagnetic susceptibility (χ_M).[81]

Synthetic details

Preparation of the representative complex $[Cu_5Dy_4O_2(OMe)_4(NO_3)_4(O_2CCH_2Bu^t)_2(pdm)_4(MeOH)_2]\cdot4MeCN\cdot1.5MeOH$ (1·4MeCN·1.5MeOH). Solids $Dy(NO_3)_3\cdot5H_2O$ (0.175 g, 0.40 mmol) and $Cu(ClO_4)_2\cdot6H_2O$ (0.185 g, 0.50 mmol) were added to a stirred yellowish solution containing H_2pdm (0.056 g, 0.40 mmol), $Bu^tCH_2CO_2H$ (25 μL, 0.20 mmol) and Et_3N (252 μL, 1.80 mmol) in a solvent mixture comprising MeCN (5 mL) and MeOH (10 mL). The resulting blue solution was stirred for a further 30 min and stored in a flask at −16 °C. X-ray quality blue crystals of the product were obtained in a period of 2 d. The crystals were collected by filtration, washed with cold MeCN (1 mL) and Et_2O (3 × 2 mL), and dried in a vacuum desiccator over anhydrous $CaCl_2$. The yield was ∼35% (based on the ligand H_2pdm available). The product was analyzed satisfactorily as lattice MeCN- and MeOH-free, *i.e.* as **1**. Anal. calcd for $C_{46}H_{70}N_8O_{32}Cu_5Dy_4$: C, 24.94; H, 3.19; N, 5.06%. Found: C, 24.83; H, 3.16; N, 5.19%. IR bands (KBr, cm^{-1}): 3425mb, 2954m, 2902w, 2866w, 1652m, 1584m, 1562s, 1468s, 1408s, 1384s, 1366m, 1340m, 1302s, 1266m, 1230m, 1162m, 1064s, 1034s, 904w, 818w, 784m, 742w, 722w, 664m, 604w, 562w, 512m, 424w. Using exactly the above mentioned procedure, but replacing $Cu(ClO_4)_2\cdot6H_2O$ with either $CuCl_2\cdot2H_2O$ (0.085 g, 0.50 mmol) or $Cu(NO_3)_2\cdot3H_2O$ (0.121 g, 0.50 mmol), gives crystals of the same product (in comparable yields), as proven by microanalyses and IR spectra.

Preparation of the complexes $[Cu_5Tb_4O_2(OMe)_4(NO_3)_4(O_2CCH_2Bu^t)_2(pdm)_4(MeOH)_2]\cdot4MeCN\cdot1.5MeOH$ (2·4MeCN·1.5MeOH) and $[Cu_5Ho_4O_2(OMe)_4(NO_3)_4(O_2CCH_2Bu^t)_2(pdm)_4(MeOH)_2]\cdot4MeCN\cdot1.5MeOH$ (3·4MeCN·1.5MeOH). These compounds were prepared in an identical manner with **1**·4MeCN·1.5MeOH by simply replacing $Dy(NO_3)_3\cdot5H_2O$ with the corresponding hydrated nitrate salts of Tb(III) and Ho(III). Typical yields were in the 30–40% range. The identity of the products was confirmed by microanalyses, IR spectra (the spectra of well dried samples of **2** and **3** are almost superimposable with the spectrum of **1** with a maximum wavenumber difference of ±5 cm^{-1}) and unit-cell determinations of their blue crystals (*vide infra*). The products were analyzed as lattice MeCN- and MeOH-free. Anal. calcd for $C_{46}H_{70}N_8O_{32}Cu_5Tb_4$ (**2**): C, 25.10; H, 3.21; N, 5.09%. Found: C, 25.24; H, 3.17; N, 5.00%. Anal. calcd for $C_{46}H_{70}N_8O_{32}Cu_5Ho_4$ (**3**): C, 24.83; H, 3.18; N, 5.04%. Found: C, 24.96; H, 3.27; N, 4.94%.

Preparation of $[Cu_5Y_4O_2(OMe)_4(NO_3)_2(O_2CCH_2Bu^t)_4(pdm)_4(MeOH)_2]\cdot2MeOH$ (4·2MeOH). Solids $Y(NO_3)_3\cdot6H_2O$ (0.077 g, 0.20 mmol) and $Cu(ClO_4)_2\cdot6H_2O$ (0.093 g, 0.25 mmol) were added to a stirred yellowish solution containing H_2pdm (0.028 g, 0.20 mmol), $Bu^tCH_2CO_2H$ (12 μL, 0.10 mmol) and Et_3N (126 μL, 0.90 mmol) in a solvent mixture comprising MeCN (4 mL) and MeOH (8 mL). The resulting blue solution was stirred for a further 30 min and stored in a flask at −16 °C. X-ray quality blue crystals of the product were obtained in a period of 2–3 d. The crystals were collected by filtration, washed with cold MeCN (1 mL) and Et_2O (2 × 2 mL), and dried in a vacuum desiccator over P_4O_{10}. The yield was ∼57% (based on the ligand H_2pdm available). The product was analyzed satisfactorily as lattice MeOH-free, *i.e.* as **4**. Anal. calcd for $C_{58}H_{92}N_6O_{30}Cu_5Y_4$: C, 34.37; H, 4.58; N, 4.15%. Found: C, 34.21; H, 4.67; N, 4.25%. IR bands (KBr, cm^{-1}): 3435mb, 2952m, 2904w, 2866m, 1652m, 1564s, 1468s, 1422s, 1401s, 1384s, 1366m, 1340m, 1302s, 1266m, 1232m, 1160m, 1066s, 1036s, 902w, 818w, 784m, 744w, 720w, 666m, 626w, 562w, 512m, 424w.

 This journal is © The Royal Society of Chemistry 2021

Open Access Article. Published on 25 November 2020. Downloaded on 2/21/2026 10:56:33 AM.
This article is licensed under a Creative Commons Attribution-NonCommercial 3.0 Unported Licence.

Single-crystal X-ray crystallography

Blue crystals of **1**·4MeCN·1.5MeOH and **4**·2MeOH were taken directly from the mother liquor and immediately cooled to −113 °C. X-ray diffraction data were collected on a Rigaku R-AXIS SPIDER Image Plate diffractometer using graphite-monochromated Mo Kα radiation. Data collection (ω-scans) and processing (cell refinement, data reduction and empirical absorption correction) were performed using the CrystalClear program package.[82] The structures were solved by direct methods using SHELXS ver. 2013/1[83] and refined by full-matrix least-squares techniques on F^2 with SHELXL ver. 2014/6.[84] H atoms were either located by difference maps and refined isotropically or were introduced at calculated positions as riding on their respective bonded atoms. All non-H atoms were refined anisotropically. The SQUEEZE procedure[85] was used for the analysis of the structure of the $\{Cu_5Dy_4\}$ cluster and the estimated additional solvents in the lattice voids are 2 MeCN and 1.5 MeOH molecules per formula unit. For compound **4**·2MeOH, one of the coordinated $Bu^tCH_2CO_2^-$ ligands has been treated as disordered. Important crystallographic data are listed in Table S1.† Full details can be found in the CIF files.

The unit cell dimensions of **2**·4MeCN·1.5MeOH and **3**·4MeCN·1.5MeOH were calculated from single-crystal diffraction measurements (Rigaku R-AXIS SPIDER Image Plate diffractometer, graphite-monochromated Mo Kα radiation). The dimensions clearly show that these two complexes are isomorphous with **1**·4MeCN·1.5MeOH. Data are as follows: **2**·4MeCN·1.5MeOH: a = 13.208(1), b = 18.964(1), c = 18.409(1) Å, $\alpha = \gamma = 90.0°$, β = 98.45(1)°, V = 4561.10(1) Å^3; **3**·4MeCN·1.5MeOH: a = 13.160(1), b = 18.910(1), c = 18.488(1) Å, $\alpha = \gamma = 90.0°$, β = 98.90(1)°, V = 4545.54 (1) Å^3. Both compounds (like **1**·4MeCN·1.5MeOH) crystallize in the monoclinic space group $I2/m$.

Conflicts of interest

There are no conflicts to declare.

Acknowledgements

A. E. and J. M. thank the Ministerio de Economia y Competitividad, Project PGC2018-094031-B-100 and PID2019-109735GB-100 for funding. S. P. P. is grateful to the COST Action: CA15128-Molecular Spintronics (MOLSPIN) for encouraging research activities in Patras. V. P. would like to thank the special Account of the NCSR "Demokritos" for financial support concerning the operation of the X-ray facilities at INN through the internal program entitled "Structural study and characterisation of crystalline materials" (NCSR "Demokritos", ELKE #10813).

Notes and references

1 C. James and P. S. Willand, *J. Am. Chem. Soc.*, 1916, **38**, 1497.
2 W. E. Bailey, R. J. Williams and W. O. Milligan, *Acta Crystallogr., Sect. B: Struct. Crystallogr. Cryst. Chem.*, 1973, **29**, 1365.
3 For example, see: A. E. Crease and P. Legzdins, *J. Chem. Soc., Dalton Trans.*, 1973, 1501.
4 J. M. Boncella and R. A. Andersen, *Inorg. Chem.*, 1984, **23**, 432.
5 O. Kahn, *Molecular Magnetism*, VCH Publishers, New York, USA, 1993.
6 *Physics of Magnetic Materials*, ed. J. Rauluszkiewics, H. Szymczak and H. K. Lachowicz, World Scientific, Singapore, 1985.
7 M. Sagawa, S. Fujimura, M. Togawa, H. Yamamoto and Y. Matsnura, *J. Appl. Phys.*, 1984, **55**, 2083.
8 For example, see: C. Edder, C. Piguet, J.-C. G. Bünzli and G. Hopfgartner, *Chem. – Eur. J.*, 2001, **7**, 3014.
9 T. Wei, S. Zhao, W. Bu, X. Lü, Y. Hui, J. Song, W.-K. Wong and R. A. Jones, *Inorg. Chem. Commun.*, 2009, **12**, 1216.
10 M. A. Subhan, T. Suzuki and J. Kaizaki, *J. Chem. Soc., Dalton Trans.*, 2002, 1416.
11 O. Margeat, P. G. Lacroix, J. P. Costes, B. Donnadieu, C. Lepetit and K. Nakatani, *Inorg. Chem.*, 2004, **43**, 4743.
12 B. Zhao, P. Cheng, X. Y. Chen, C. Cheng, W. Shi, D. Z. Liao, S. P. Yan and Z. H. Jiang, *J. Am. Chem. Soc.*, 2004, **126**, 3012.
13 E. Loukopoulos, K. Griffiths, G. R. Akien, N. Kourkoumelis, A. Abbul-Sada and G. E. Kostakis, *Inorganics*, 2015, **3**, 448.
14 C. Benelli and D. Gatteschi, *Chem. Rev.*, 2002, **102**, 2369.
15 G. Condorelli, I. Fragala, S. Giuffrida and A. Cassol, *Z. Anorg. Allg. Chem.*, 1975, **251**, 412.
16 A. Bencini, C. Benelli, A. Caneschi, R. L. Carlin, A. Dei and D. Gatteschi, *J. Am. Chem. Soc.*, 1985, **107**, 8128.
17 A. Bencini, C. Benelli, A. Caneschi, A. Dei and D. Gatteschi, *Inorg. Chem.*, 1986, **25**, 572.
18 N. Matsumoto, M. Sakamoto, H. Tamaki and H. Okawa, *Chem. Lett.*, 1990, 853.
19 O. Kahn, *Struct. Bonding*, 1987, **68**, 69.
20 C. Benelli, A. Caneschi, D. Gatteschi, O. Guillou and L. Pardi, *Inorg. Chem.*, 1990, **29**, 1570.
21 M. Andruh, I. Ramade, E. Codjovi, O. Guillou, O. Kahn and J. C. Trombe, *J. Am. Chem. Soc.*, 1993, **115**, 1822.
22 O. Kahn and O. Guillou, *Res. Front. Magnetochem.*, 1993, 179.
23 R. E. P. Winpenny, *Chem. Soc. Rev.*, 1998, **27**, 447.
24 F. Hulliger, M. Landolt and H. Vetsch, *J. Solid State Chem.*, 1976, **18**, 283.
25 For an early review, see: G. Aromi and E. K. Brechin, *Struct. Bonding*, 2006, **122**, 1.
26 R. Bagai and G. Christou, *Chem. Soc. Rev.*, 2009, **38**, 1011.
27 M. Evangelisti and E. K. Brechin, *Dalton Trans.*, 2010, **39**, 4672 (Dalton Perspective), and references therein.
28 Y.-Z. Zheng, G.-J. Zhou, Z. Zheng and R. E. P. Winpenny, *Chem. Soc. Rev.*, 2014, **43**, 1462.
29 R. Sessoli, D. Gatteschi, A. Caneschi and M. A. Novak, *Nature*, 1993, **365**, 141.
30 R. Sessoli, H.-L. Tsai, A. R. Schake, S. Wang, J. B. Vincent, K. Folting, D. Gatteschi, G. Christou and D. N. Hendrickson, *J. Am. Chem. Soc.*, 1993, **115**, 1804.

Open Access Article. Published on 25 November 2020. Downloaded on 2/21/2026 10:56:33 AM.
This article is licensed under a Creative Commons Attribution-NonCommercial 3.0 Unported Licence.

31 C. J. Milios and R. E. P. Winpenny, *Struct. Bonding (Berlin)*, 2015, **164**, 1.
32 N. Ishikawa, M. Sugita, T. Ishikawa, S.-Y. Koshihara and Y. Kaizu, *J. Am. Chem. Soc.*, 2003, **125**, 8694.
33 S. T. Liddle and J. van Slageren, *Chem. Soc. Rev.*, 2015, **44**, 6655.
34 D. N. Woodruff, R. E. P. Winpenny and R. A. Layfield, *Chem. Rev.*, 2013, **113**, 5110.
35 F.-S. Guo, B. M. Day, Y.-C. Chen, M.-L. Tong, A. Mansikkamäki and R. A. Layfield, *Science*, 2018, **362**, 1400.
36 K. Liu, W. Shi and P. Cheng, *Coord. Chem. Rev.*, 2015, **289–290**, 74.
37 For a review, see: A. Dey, J. Acharya and V. Chandrasekhar, *Chem. – Asian J.*, 2019, **14**, 4433.
38 For a minireview, see: A. Chakraborty, J. Goura, P. Bag and V. Chandrasekhar, *Eur. J. Inorg. Chem.*, 2019, 1180.
39 For a perspective, see: L. R. Piquer and E. C. Sañudo, *Dalton Trans.*, 2015, **44**, 8771.
40 J. W. Sharples and D. Collison, *Coord. Chem. Rev.*, 2014, **260**, 1.
41 H. L. C. Feltham and S. Brooker, *Coord. Chem. Rev.*, 2014, **276**, 1.
42 Y. Peng, M. K. Singh, V. Mereacre, C. E. Anson, C. Rajaraman and A. K. Powell, *Chem. Sci.*, 2019, **10**, 5528.
43 R. Sessoli and A. K. Powell, *Coord. Chem. Rev.*, 2009, **253**, 2328.
44 C. D. Polyzou, C. G. Efthymiou, A. Escuer, L. Cunha-Silva, C. Papatriantafyllopoulou and S. P. Perlepes, *Pure Appl. Chem.*, 2013, **85**, 315.
45 Z. G. Lada, E. Katsoulakou and S. P. Perlepes, in *Single-Molecule Magnets: Molecular Architectures and Building Blocks for Spintronics*, ed. M. Holyńska, Wiley-VCH, Weinheim, Germany, 2019, pp. 245–313.
46 H. Li, Z.-J. Yao, D. Liu and G.-X. Jin, *Coord. Chem. Rev.*, 2015, **293–294**, 139.
47 S. K. Langley, B. Moubaraki, C. Tomasi, M. Evangelisti, E. K. Brechin and K. S. Murray, *Inorg. Chem.*, 2014, **53**, 13154.
48 J. Wu, L. Zhao, M. Guo and J. Tang, *Chem. Commun.*, 2015, **51**, 17317.
49 J. Wu, L. Zhao, L. Zhang, X.-L. Li, M. Guo, A. K. Powell and J. Tang, *Angew. Chem., Int. Ed.*, 2016, **55**, 15774.
50 J. Wu, X.-L. Li, M. Guo, L. Zhao, Y.-Q. Zhang and J. Tang, *Chem. Commun.*, 2018, **54**, 1065.
51 D. Dermitzaki, G. Lorusso, C. P. Raptopoulou, V. Psycharis, A. Escuer, M. Evangelisti, S. P. Perlepes and T. C. Stamatatos, *Inorg. Chem.*, 2013, **52**, 10235.
52 D. Dermitzaki, C. P. Raptopoulou, V. Psycharis, A. Escuer, S. P. Perlepes and T. C. Stamatatos, *Inorg. Chem.*, 2015, **54**, 7555.
53 For example, see: T. C. Stamatatos, G. C. Vlahopoulou, C. P. Raptopoulou, A. Terzis, A. Escuer and S. P. Perlepes, *Inorg. Chem.*, 2009, **48**, 4610.
54 For example, see: T. Taguchi, T. C. Stamatatos, K. A. Abboud, C. M. Jones, K. M. Poole, T. A. O'Brien and G. Christou, *Inorg. Chem.*, 2008, **47**, 4095.
55 For example, see: M. Murugesu, M. Habrych, W. Wernsdorfer, K. A. Abboud and G. Christou, *J. Am. Chem. Soc.*, 2004, **126**, 4766.
56 For example, see: K. I. Alexopoulou, C. P. Raptopoulou, V. Psycharis, A. Terzis, V. Tangoulis, T. C. Stamatatos and S. P. Perlepes, *Aust. J. Chem.*, 2012, **65**, 1608.
57 D. Alexandropoulos, L. Cunha-Silva, L. Pham, V. Bekiari, G. Christou and T. C. Stamatatos, *Inorg. Chem.*, 2014, **53**, 3220.
58 P.-P. Yang, *Z. Anorg. Allg. Chem.*, 2011, **637**, 1234.
59 P.-P. Yang, X.-F. Gao, H.-B. Song, S. Zhang, X.-L. Mei, L.-C. Li and D.-Z. Liao, *Inorg. Chem.*, 2011, **50**, 720.
60 M. Murugesu, A. Mishra, K. A. Abboud, G. Christou and W. Wernsdorfer, *Polyhedron*, 2006, **25**, 613.
61 X.-Q. Zhao, Y. Lan, B. Zhao, P. Cheng, C. E. Anson and A. K. Powell, *Dalton Trans.*, 2010, **39**, 4911.
62 T.-X. Lan, W.-S. Gao, C.-N. Chen, H.-S. Wang, W. Wang and Y.-H. Fan, *New J. Chem.*, 2018, **42**, 5798.
63 T. N. Hooper, R. Inglis, G. Lorusso, J. Ujma, P. E. Barran, D. Uhrin, J. Schnack, S. Piligkos, M. Evangelisti and E. K. Brechin, *Inorg. Chem.*, 2016, **55**, 10535.
64 T. N. Hooper, R. Inglis, M. A. Palacios, G. S. Nichol, M. B. Pitak, S. J. Coles, G. Lorusso, M. Evangelisti and E. K. Brechin, *Chem. Commun.*, 2014, **50**, 3498.
65 F. A. Cotton, G. Wilkinson, C. A. Murillo and M. Bochmann, *Advanced Inorganic Chemistry*, 6th edn, Wiley, New York, 1999, p. 1109.
66 W. J. Evans, J. L. Shreeve, J. W. Ziller and R. J. Doedens, *Inorg. Chem.*, 1995, **34**, 576.
67 P. C. Junk, D. L. Kepert, B. W. Skelton and A. H. White, *Aust. J. Chem.*, 1999, **52**, 497.
68 A. K. Boudalis, V. Nastopoulos, A. Terzis, C. P. Raptopoulou and S. P. Perlepes, *Z. Naturforsch.*, 2001, **56b**, 122.
69 A. W. Addison, T. N. Rao, J. Reedijk, J. Rijn and G. C. Verschoor, *J. Chem. Soc., Dalton Trans.*, 1984, 1349.
70 M. Llunell, D. Casanova, J. Girera, P. Alemany and S. Alvarez, *SHAPE, version 2.0*, Barcelona, Spain, 2010.
71 D. Dermitzaki, C. P. Raptopoulou, V. Psycharis, A. Escuer, S. P. Perlepes and T. C. Stamatatos, Unpublished results.
72 V. Mereacre, A. M. Ako, R. Clérac, W. Wernsdorfer, I. J. Hewitt, C. E. Anson and A. K. Powell, *Chem. – Eur. J.*, 2008, **14**, 3577.
73 S. K. Langley, N. F. Chilton, B. Moubaraki, T. Hooper, E. K. Brechin, M. Evangelisti and K. S. Murray, *Chem. Sci.*, 2011, **2**, 1166.
74 S. K. Langley, L. Ungur, N. F. Chilton, B. Moubaraki, L. F. Chibotaru and K. S. Murray, *Chem. – Eur. J.*, 2011, **17**, 9209.
75 T. Rajeshkumar, H. V. Annadata, M. Evangelisti, S. K. Langley, N. F. Chilton, K. S. Murray and G. Rajaraman, *Inorg. Chem.*, 2015, **54**, 1661.
76 J. Wu, L. Zhao, L. Zhang, X.-L. Li, M. Guo and J. Tang, *Inorg. Chem.*, 2016, **55**, 5514.
77 M. Coletta, R. McLellan, S. Sanz, K. J. Gagnon, S. J. Teat, E. K. Brechin and S. J. Dalgarno, *Chem. – Eur. J.*, 2017, **23**, 14073.

This journal is © The Royal Society of Chemistry 2021

Open Access Article. Published on 25 November 2020. Downloaded on 2/21/2026 10:56:33 AM.
This article is licensed under a Creative Commons Attribution-NonCommercial 3.0 Unported Licence.

78 F. Shao, J.-J. Zhuang, M.-G. Chen, N. Wang, H.-Y. Shi, J.-P. Tong, G. Luo, J. Tao and L.-S. Zheng, *Dalton Trans.*, 2018, **47**, 16850.
79 N. F. Chilton, R. P. Anderson, L. D. Turner, A. Soncini and K. S. Murray, *J. Comput. Chem.*, 2013, **34**, 1164.
80 J. Bartolomé, G. Filoti, V. Kuncser, G. Schinteie, V. Mereacre, C. E. Anson, A. K. Powell, D. Prodius and C. Turta, *Phys. Rev. B: Condens. Matter Mater. Phys.*, 2009, **80**, 014430.
81 G. A. Bain and J. F. Berry, *J. Chem. Educ.*, 2008, **85**, 532.
82 *CrystalClear*, Rigaku/MSC Inc., The Woodlands, TX, USA, 2005.
83 G. M. Sheldrick, *Acta Crystallogr., Sect. A: Fundam. Crystallogr.*, 2008, **64**, 112.
84 G. M. Sheldrick, *Acta Crystallogr., Sect. C: Cryst. Struct. Commun.*, 2015, **71**, 3.
85 A. L. Spek, *Acta Crystallogr., Sect. C: Cryst. Struct. Commun.*, 2015, **71**, 9.